PHYSICAL REVIEW B VOLUME 43, NUMBER 5 15 FEBRUARY 1991-I

Defect relaxation in amorphous silicon: Stretched exponentials, the Meyer-Neldel rule, and the Staebler-Wronski effect

Richard S. Crandall
Solar Energy Research Institute, Golden, Colorado 80401
(Received 3 August 1990; revised manuscript received 28 September 1990)

Annealing and production of metastable defects in disordered solids is explained quantitatively with a model in which defect relaxation is a local phenomenon. The stretched-exponential time dependence of defect relaxation and the Meyer-Neldel rule for the relaxation-time constant are natural consequences of this model. The results are obtained by using an exponential distribution of activation barriers for transitions between the two states of the local defect. The model, applied to data in hydrogenated amorphous silicon, *a*-Si:H, gives an exponential distribution of barriers with a characteristic temperature of 220 °C, roughly equal to the accepted freeze-in temperature for defect distributions in *a*-Si:H. The model explains that long degradation times convert defects with higher barriers and this results in longer annealing times. The microscopic models of the metastable defects in *a*-Si:H, weak-bond breaking and carrier trapping by charged dangling bonds, are discussed in the framework of this defect-relaxation model.

I. INTRODUCTION

A. Aims

This paper presents a model for the kinetics of annealing and production of metastable defects (MSD) in disordered solids with specific application to amorphous silicon. I use a model of defect-controlled relaxation (DCR) in which an ensemble of local defects relaxes *without* the aid of a diffusing atom. Each defect may consist of more than a single atom. The model gives a stretched-exponential[1] time dependence for defect relaxation and predicts that defect annealing or production obey a Meyer-Neldel (*MN*) rule.[2] I contrast this model with the hydrogen-diffusion-controlled defect-relaxation (HCR) model[3] and show that the HCR and DCR models both explain most experimental data. These models give similar results because the defect relaxation kinetics are governed by the underlying disorder of the amorphous solid. However, some predictions of the DCR model, not found in the HCR model, are supported by experiment.

B. Background

Twelve years ago Staebler and Wronski[4] observed a metastable decrease in the photoconductivity and dark conductivity of hydrogenated amorphous silicon (*a*-Si:H) following prolonged illumination. These changes, known as the Staebler-Wronski (SW) effect, can be completely removed by annealing at elevated temperature. There is intense interest in this and related metastable effects such as light-induced changes of the $g=2.0055$ electron spin resonance (ESR) (Ref. 5) and luminescence,[6,7] in undoped *a*-Si:H, of junction capacitance of devices,[8] and of solar-cell efficiency.[9] Most of these metastable changes can also be produced by charge injection.[9,10] Reverse-bias annealing-induced conductivity increases,[11] and bias-induced threshold voltage shifts in thin-film transistors[12] (TFT's) are also observed.

Quenched in conductivity increases[3,13] or ESR signal[14] have received considerable attention recently. These reversible changes are believed to be connected with the same defect or mechanism responsible for the SW effect. They are produced by raising the film temperature above a defect equilibrium temperature and then quenching to room temperature. The increases can be completely reduced by raising the sample above the equilibration temperature and then cooling slowly to room temperature.

Metastabilities occur in all types of *a*-Si:H and its alloys and have recently been observed in crystalline silicon solar cells.[15] In addition to their considerable scientific interest, they are of significant technological interest because they result in the reversible light-induced degradation of *a*-Si:H solar cells and threshold voltage shifts in TFT's. As yet there is no universally accepted model for these phenomena.

1. Macroscopic models

Many models for the SW effect have been presented. Most are variations on two basic microscopic models. These are the weak-bond breaking and the charge-trapping defect model. Both explain most of the experimental data and result in the same final metastable state *B*; that is a neutral threefold-coordinated dangling-bond defect (T_3^0). This defect, since it is neutral and located near midgap, is an excellent recombination center which decreases the photoconductivity. Its unpaired spin increases the ESR signal.[5] The increase in the 0.95-eV defect luminescence band[6] is also explained by an increase in these defects. These defects also compete with the normal 1.2-eV band-tail–band-tail luminescence and reduce its intensity. However, the models postulate different an-

nealed states, A, and the mechanism leading to state B. The two models are outlined below.

Weak bond. The earliest microscopic mechanism proposed to explain the SW effect was light-induced breaking of weak Si—Si bonds. Various authors[6,16,17] suggest that a defect is created when a weak or highly strained Si—Si bond is broken following the absorption of a photon. The photon promotes an electron from a bonding orbital to an antibonding orbital followed by nonradiative recombination of the electron and hole. The recombination energy breaks the bond between the fourfold-coordinated neutral Si atoms (T_4^0). This results in two neighboring T_3^0, thus explaining the increase in the ESR signal.

Breaking a weak bond is a multistep process. Stutzmann describes the energy balance for this process by comparing the energies of the weak-bond state and the final state containing two dangling bonds.[18,19] He lists various excitations of the weak bond resulting in lower final than initial energies. These include (i) illumination resulting in excitation of an electron from a bonding to an antibonding orbital on the weak bond, and (ii) charge injection resulting in two holes or two electrons on a weak bond. In process (i) the final energy is 0.4 eV less than the initial energy; thus the weak bond should break. Process (ii) results in no energy change, so the bond may or may not break. In both cases the details of the bond breaking are neglected. Local atomic rearrangement between the weak bond and two dangling bonds certainly forms a potential barrier of unknown magnitude. This may well be the rate-limiting step for any transition.

Stabilization and/or separation of the dangling bonds is a crucial step. Dersch *et al.*[5] and Morigaki *et al.*[7] postulate that a neighboring H atom changes its position to separate the two dangling bonds. In this model, the photon energy must be transferred to a local mode both to break the Si—Si bond and to move the bonded H to stabilize and separate the two dangling bonds. Defect annealing is the reverse of its formation. The hydrogen atom moves away, permitting the two dangling bonds to face each other and recombine. It is not clear that the energy available after the electron and hole have thermalized is sufficient to break the weak bond and move the hydrogen.[20] Based on their experiments with MSD defect production by quenching from elevated temperature, Kakalios *et al.*[3] expanded this model to include the breaking of the Si—H bond and diffusion of the H atom to (away from) the weak-bond site to produce (anneal) the MSD. Their rational for this H diffusion-controlled model was the correlation between dispersive hydrogen diffusion and MSD annealing. Stutzmann *et al.*[21] experimentally investigated some of the models for the role of hydrogen and concluded that if hydrogen were involved in the weak-bond breaking, it could not be the rate-limiting step.

This weak-bond model, however, does not explain the decrease in electrical conductivity in doped a-Si:H. The weak bond contains two states that lie below the Fermi level. The two T_3^0 that are formed also contain two states below the Fermi level. Thus no states are moved from above to below the Fermi to decrease the conductivity, as required to explain the SW effect.[22]

Charged dangling bond. Adler[22] proposed an alternative to the weak-bond model. The model requires that at least 10^{17} cm^{-3} threefold-coordinated negative and positive charged dangling bond defects (T_3^- and T_3^+) exist in undoped a-Si:H. Since these defects relieve local strain they can exist in large numbers. He[22] postulated that T_3 is negatively correlated in certain strained regions of a-Si:H, so a large number of charged dangling bonds form in undoped a-Si:H. Of course, the correlation energy cannot be negative everywhere, because undoped a-Si:H contains at least 10^{15} cm^{-3} unpaired spins that are believed to be due to the neutral dangling bonds on T_3^0 defects.

During illumination with band-gap light, electrons and holes, respectively, are trapped on the T_3^+ and T_3^- defects. This forms neutral defect centers, but without rehybridization or relocation of the neighboring atoms. Since the electronic levels of the trapped carriers are near band edges, these defects are readily thermally ionized back to T_3^+ and T_3^- except at low temperature. However, there is a small probability of rehybridization to make a stable dangling bond. Since the T_3^+ and T_3^- have different bond angles than the T_3^0, a lattice relaxation is necessary to stabilize the neutral dangling bond. The 15° bond-angle change is expected to move the defects' electronic level from near a band edge toward midgap, where it functions as a more efficient recombination center and appears as a stable T_3^0.[23]

Metastable defect annealing is the thermal excitation of a charge from the T_3^0 together with lattice relaxation to reform the native T_3^+ or T_3^-. The annealing energy of each defect is independent and related to the different electronic transition energies[24] of the T_3^0. The ionization of an electron from a T_3^0 to the conduction band requires less energy than the ionization of a hole to the valence band.[24] Apart from this difference, there may be differences in the energy of relaxation back to the charged defects. Charge-sensitive measurements of annealing of metastable defects in a large number of solar-cell devices show that the annealing energy for hole removal is always a few tenths of an electron volt higher than for electron removal,[25] in support of this model.

Recent thermodynamic models of inhomogeneous a-Si:H with a *positive* correlation energy also predict large numbers of charged dangling bonds.[26,27] Branz and Silver[27] show that positively correlated charged dangling-bond defects can exist in large numbers due to short-range potential fluctuations. These potential fluctuations arise from inhomogeneities in the a-Si:H on the length scale of 5–30 Å. The T_3^+ are electron traps near the conduction-band edge; the T_3^- are hole traps near the valence-band edge. This model allows T_3^+ and T_3^- to coexist with T_3^0 in spite of a positive correlation energy. Branz[24] reinterpreted recent infrared ESR measurements of Ristein *et al.*[28] on a-Si:H containing roughly 10^{16} cm^{-3} T_3^0 defects to indicate the presence of about 10^{17} cm^{-3} of T_3^+ and T_3^-. Recent depletion width modulated-ESR measurements of Essick and Cohen[29] also appear to suggest that there are more T_3^- than T_3^0 defects in undoped a-Si:H.[23,24] Shimizu *et al.*,[30] using a combination of constant-photocurrent-method absorp-

tion and light-induced ESR (LESR), also show that many charged defects are present in undoped a-Si:H.

If charge-trapping defects exist in a-Si:H they can be understood in analogy with crystalline materials, where charge-trapping defect reactions are well known. Bistable charge-state-controlled defects have been observed in a variety of doped crystalline semiconductors.[31] These defects, described by a two-level system, change their stable configuration with their charge state. A substantial barrier, as much as 0.64 eV for the iron-acceptor defect in Si,[32] retards these configurational changes. Branz[24] describes metastable conductivity changes observed by quenching from high temperature, illuminating, or charge-depleting doped amorphous silicon in terms of bistable charge-trapping reactions involving the dopant atoms. Whenever a charge-sensitive measuring technique[25,33] is used to study MSD in a-Si:H, a charge change is observed as the defect makes the transition from the annealed to the degraded state. These results suggest the Staebler-Wronski and other metastable effects may involve bistable charge-trapping defects, such as T_3^+ and T_3^-.

2. Experiments

Production kinetics. The kinetics of light-induced defect production at room temperature was given a quantitative explanation by Stutzmann *et al.*[34,35] They measured the kinetics of light-induced defect formation and found that the number of defects increased roughly as the cube root of the time (t). They explained their data using a model in which optically excited electron-hole pairs nonradiatively recombine from band tail to band tail and break weak Si—Si bonds. The sublinear $t^{+1/3}$ time dependence results because of the increasing number of T_3^0 defects that produce an alternative pathway for electron-hole recombination. Of course, this explanation also applies to the Adler model of the metastability.

Redfield and Bube[36] find that a stretched exponential fits published data of light-induced MSD production as well as does the $t^{1/3}$ dependence originally modeled by Stutzmann *et al.*[34,35] Redfield and Bube postulate a rate equation based on that of Kakalios *et al.*[3] using the HCR model. Redfield and Bube do not specify the physics underling their rate equation. If they envision the HCR model, the light would have to excite hydrogen motion. However, there is no evidence for light-induced hydrogen motion at room temperature.

Other experiments have implicated charge-trapping reactions.[10,12,25,33,37] These experiments show that recombination is not necessary, because degradation can be induced by single charge injection in device structures. The annealing kinetics are the same as for light-induced degradation, implying that the same MSD's are produced by single charge injection as light.

The literature regarding the thermal activation energy for light-induced MSD production separates in two parts. Near room temperature, a low thermal activation energy is observed. Lee *et al.*[38] and Stutzmann *et al.*[34,35] find $E_{act} \approx 0.04$ eV for dangling-bond production observed by ESR, and Nickel *et al.*[39] find $E_{act} = 0.06$ eV for shifts in the threshold voltage in a TFT structure. However, at higher temperature (>100 °C), $E_{act} \approx 1$ eV.[10,25] These high-temperature results show that states A and B are separated by an energy barrier on the order of 1 eV.

Measurements involving single charge injection always show thermally activated MSD production with E_{act} on the order of 1 eV. Nickel et al.[39] injected charge in amorphous silicon TFT structures to produce MSD's, and find $E_{act} = 0.7$ eV. Similar results are obtained by Hepburn *et al.*[12] Jackson and Moyer[33] injected charge in a-Si:H/a-Si:N:H heterojunctions and find $E_{act} = 1.1$ eV. They also show that defect production in heterojunctions obeys a stretched exponential. Although they analyzed their data in terms of a HCR, it can equally well be described by the DCR model, as I show later. Using electron injection in a variety of p-i-n and Schottky-barrier solar cells, I find activation energies ranging from 0.6 to 1.1 eV in the temperature range above 370 K.[10,25]

Thus one may conclude that light supplies, by some mechanism, the energy to surmount the energy barrier between states A and B. At low temperature, it is the dominant mechanism for producing the transition. Nevertheless, at high temperature, thermal energy is more important, so that a thermally activated process with a high activation energy can be observed.

Annealing kinetics. Considerable data on the annealing kinetics of the MSD are available. I surveyed most of the literature for annealing kinetics, and summarize the data in Fig. 1, in terms of the annealing activation energy (E_{act}) and the preexponential factor (ν) of the annealing rate $R_a = \nu \exp(-E_{act}/k_B T)$. The absolute temperature

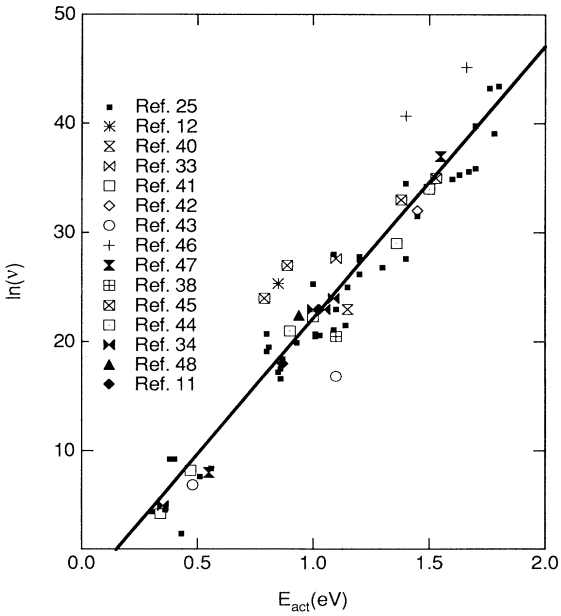

FIG. 1. Natural logarithm of the pre-exponential factor ν plotted vs the activation energy for annealing for a variety of different expeirments.

is T, and Boltzmann's constant is k_B. This type of plot shows that the data[11,12,25,33,34,38,40–48] obey a Meyer-Neldel rule of the form $\ln(\nu) \propto E_{\rm act}$. It is remarkable that these data, from a wide variety of measurements on doped and undoped a-Si:H, are distributed along a straight line. From this, one is tempted to say there is a common defect for all the metastable effects. However, this behavior does not mean there is a common defect, only that the measurements reflect an underlying disorder common to all defects in amorphous silicon. In this article I show how the disorder permits different defects to exhibit similar annealing behavior. Most samples in Fig. 1 are represented by a single point. Nevertheless, some samples exhibit two distinct annealing energies. In Fig. 2, I replot the data from samples exhibiting multiple annealing energies.[45,46]

Most of the data in Fig. 2 are for p-i-n devices, where the charge state of the defect is measured by transient capacitance.[25] Both electron-and hole-containing defects have been observed in the same sample. The electron-containing MSD anneals with $E_{\rm act} \leq 1.2$ eV, as it loses an electron. The hole-emitting MSD's have $E_{\rm act} \geq 1.35$ eV. Nevertheless, both lie along the same Meyer-Neldel rule line.

Other points in Fig. 2 are for conductivity measurements, which show both an increase and decrease on a single sample. These changes anneal with different activation energies. Measurements by Deng and Fritzsche[49] showing this phenomenon in phosphorous-doped a-Si:H are reproduced in Fig. 3. Following light-induced degradation, the conductivity is depressed as in the SW effect. However, during annealing, the conductivity returns to its state A value and then continues to increase. Finally, this increase anneals away, and the conductivity returns to its fully annealed value. This phenomenon has also been observed in p-type[45] and compensated material.[46] In all cases, the conductivity increase has the higher annealing activation energy.

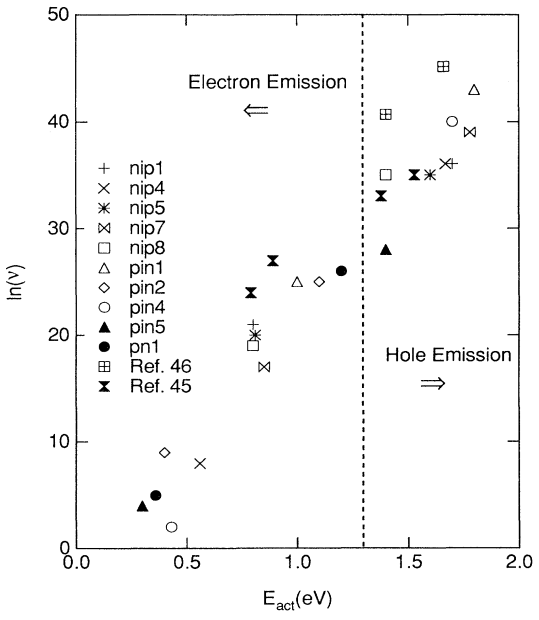

FIG. 2. The data labeled by n-i-p, p-i-n, or p-n are for annealing data determined from capacitance transients (Ref. 25). The data labeled by reference number are for conductivity changes. Arrows indicate regions where electron or hole emission is observed during defect annealing.

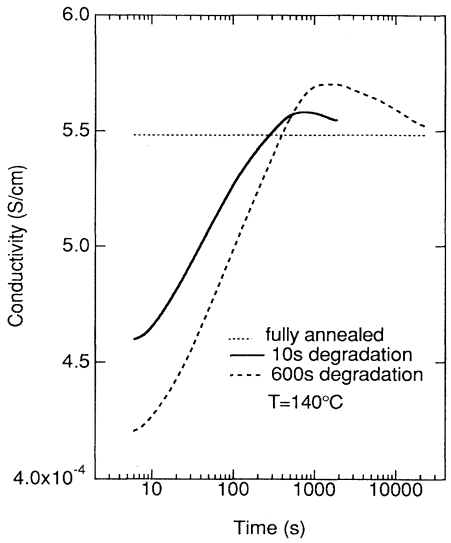

FIG. 3. Annealing of conductivity for a lightly phosphorous-doped sample following 10-s and 10-min degradations. Data from Fig. 5 of Ref. 49. The dotted line is the fully annealed value.

These two conductivity or charge changes that anneal with distinct activation energies show that there are two distinct defects in a-Si:H. This result is consistent with the charged dangling-bond model, but is hard to explain with the weak-bond model.

3. *Recent models of defect relaxation kinetics*

Hydrogen diffusion controlled. The Xerox group[3,33,48] postulated that the rate-limiting step in MSD formation or annealing is hydrogen diffusion. They view each metastable defect reaction as a hydrogen-diffusion-controlled reaction. Street *et al.*[50] discovered that the hydrogen diffusion coefficient is time dependent. They connect this result to MSD annealing by assuming that the annealing rate is determined by the time dependence of the hydrogen-diffusion coefficient. This yields a time-dependent rate equation for MSD relaxation. The solution of the resulting rate equation is a stretched exponential, consistent with the experimentally observed annealing kinetics of MSD's. Jackson[51] used the idea of dispersive transport of hydrogen (analogous to that of multiple-trapping carrier transport in a-Si:H) to derive a Meyer-Neldel rule for defect annealing. In this HCR model, the random walk of the hydrogen through an exponential distribution of trapping sites is the key to un-

derstanding the defect-relaxation kinetics. In order for this model to be consistent with its fundamental premise that it is the *macroscopic* hydrogen motion, as measured by the diffusion experiments, the hydrogen atom must move a macroscopic distance during defect relaxation.

Defect controlled. A second class of models supposes that the defect itself, rather than the diffusion of another atom to it, controls the reaction kinetics. An internal barrier to defect reconfiguration determines the rates of creation or annealing in these defect-controlled reactions.[52,53] Defect annealing or production in the weak-bond or charged dangling-bond models could be a DCR. All metastable defects in crystalline solids certainly exhibit a DCR because there is no mobile species to determine nonlocal kinetics.

An example of a DCR that gives a stretched-exponential relaxation is electron emission in anthracene. Campos *et al.*[54] used an exponential distribution of traps that decrease in number from the conduction-band edge toward midgap to derive this rate law. However, they do not connect this to the MN rule. Dyer[55] uses a general phenomenological model with the same exponential distribution to derive a Meyer-Neldel rule for electron transport in disordered material.

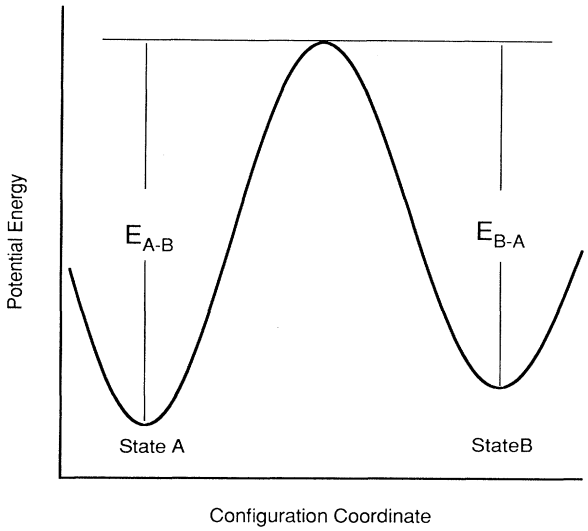

FIG. 4. Configuration coordinate diagram of a MSD. Energies are defined in the text.

C. Paper outline

In this paper, I present a brief outline of the derivation of a stretched-exponential relaxation based on the DCR model and show how this leads to a MN rule for production or annealing of MSD. Section II develops the general mathematical formalism for defect-controlled relaxation. In Sec. III, I compare the results with experimental data and the HCR model. The two main microscopic models of the Staebler-Wronski effect are discussed in terms of the DCR and HCR models in Sec. IV. Section V summarizes the paper.

II. DEFECT-CONTROLLED RELAXATION MODEL

The results of this section were briefly presented elsewhere.[52,53] In this paper, details of the calculation are given, as well as predictions of the model and comparison with experiment and the microscopic defect models.

A. Two-level system

The transitions involved in MSD production and annealing can be understood with reference to the two-level configuration coordinate diagram shown in Fig. 4. In this representation, a MSD is either state A or B. Since defect production leads to a saturated value of defects on the order of $10^{+17}\ \mathrm{cm}^{-3}\,\mathrm{eV}^{-1}$,[56] I consider that there are a finite number (N_D) of defects. In equilibrium, most of the defects are in state A. The barrier to the transition between states is a one-dimensional representation of a multidimensional configuration space, through which the defect passes during the transition. The energy axis shows the enthalpy rather than the free energy. In reality, one should consider the free-energy change in the transition from state A to B.[57] In this paper, I neglect any entropy change of an individual defect in the transition. The transition from state A to state $B(A \Longrightarrow B)$ proceeds over the barrier of height $E_{A\text{-}B}$ and the transition from state B to state $A(B \Longrightarrow A)$ proceeds over the barrier $E_{B\text{-}A}$.

In an amorphous material disorder produces a variation in barrier heights and energy minima among different defect sites. The ground-state energy and the metastable minimum can also vary among the different defects. However, I consider only a distribution of barrier heights, $E_{B\text{-}A}$ and $E_{A\text{-}B}$. Each individual defect, however, has a well-defined energy barrier. In contrast, an ensemble of MSD's in a crystalline material is composed of equivalent defects, so there is a single well-defined energy barrier for each process.

Thermodynamic equilibrium arguments[26] show how exponential defect distributions, characterized by the temperature T^*, result when defects are frozen in when cooling below T^*. Since defects are in thermodynamic equilibrium above T^*, their distribution is given by a Boltzmann expression of the form $N_{\mathrm{def}}=N_0\exp(-F/k_BT^*)$. F is the Gibbs free energy of formation of the defect, and N_0 is the number of defect sites. Below T^*, thermodynamic equilibrium cannot be maintained, so that the defect distribution reflects that at T^*. Examples include both band tails.[26]

An extension of the above arguments suggests that all defects will be distributed exponentially in energy. I assume that the energy barrier mirrors the formation energy. In principal, defect distributions could be exponentially increasing or decreasing functions of the barrier height. If the defect density *decreases* with barrier height, then the model of Campos *et al.*[54] shows that defect relaxation will be characterized by a stretched-exponential time dependence. If the defect density *increases* with barrier height, then the calculation below

shows that defect relaxation is also characterized by a stretched-exponential time dependence. However, as I point out later, these two different model distributions lead to slight differences in MSD annealing behavior.

For purposes of the calculation below, I assume that defects with the highest barriers have the lowest formation energy, and use the height of the energy barrier to parameterize the defect. The ith defect in the ensemble is characterized by a barrier energy E_i. This barrier height depends on the direction of the transition; i.e., $E_i = E_{A\text{-}B}$ for the transition $A \Longrightarrow B$, and $E_i = E_{B\text{-}A}$ for $B \Longrightarrow A$. The barrier heights are assumed to extend from some minimum value to a maximum of E_{mA} for $E_{A\text{-}B}$ and E_{mB} for $E_{B\text{-}A}$.

B. Rate equation and Meyer-Neldel rule

The time rate of conversion of MSD from one state to the other is given by an elementary first-order rate equation. The density of defects in state A per unit volume per unit energy at energy E_i is $n_A(E_i)$; the density in state B is $n_B(E_i)$. The transition probability per unit time per defect from state A to B is $W_{A\text{-}B}(E_i)$; for B to A it is $W_{B\text{-}A}(E_i)$. The rate of change of $n_A(E_i)$ or $n_B(E_i)$ is

$$\frac{dn_A(E_i)}{dt} = -\frac{dn_B(E_i)}{dt} = -n_A(E_i)W_{A\text{-}B}(E_i) + n_B(E_i)W_{B\text{-}A}(E_i) \ . \tag{1}$$

The first term on the right-hand side of Eq. (1) is the rate of transition $A \Longrightarrow B$. The second term, the rate of transition $B \Longrightarrow A$, represents annealing. Most probes of the defect density are not energy specific. They only measure the total number of defects in a particular state. The total population in states A and B are, respectively,

$$N_A(t) = \sum_i n_A(E_i); \quad N_B(t) = \sum_i n_B(E_i) \ . \tag{2}$$

Using Eqs. (1) and (2), the rate of change of $N_A(t)$ or $N_B(t)$ is

$$\frac{dN_A(t)}{dt} = -\frac{dN_B(t)}{dt} = \sum_i [-n_A(E_i)W_{A\text{-}B}(E_i) + n_B(E_i)W_{B\text{-}A}(E_i)] \ . \tag{3}$$

Since I assume that the states are distributed continuously in energy, the summation is converted to an integration over the barrier energy E. The assumed exponential distribution functions for states A and B, respectively, are

$$\frac{dn_A(E)}{dE} = \kappa_A e^{+E/k_BT^*} \quad \text{and} \quad \frac{dn_B(E)}{dE} = \kappa_B e^{E/k_BT^*} \ , \tag{4}$$

where κ_A and κ_B are normalization constants, determined from Eq. (2). They are

$$\kappa_A = \frac{N_A(t)}{k_BT^*} e^{-E_{mA}/k_BT^*} \quad \text{and} \quad \kappa_B = \frac{N_B(t)}{k_BT^*} e^{-E_{mB}/k_BT^*} \ , \tag{5}$$

where E_{mA} and E_{mB} are the maximum barrier heights defined above. Using the assumed distribution functions and passing to the continuum limit, Eq. (3) becomes

$$\frac{dN_A(t)}{dt} = -N_A(t)\int_{E_1}^{E_{mA}} \frac{dE}{k_BT^*} W_{A\text{-}B}(E) e^{-(E_{mA}-E)/k_BT^*} + N_B(t)\int_{E_1}^{E_{mB}} \frac{dE}{k_BT^*} W_{B\text{-}A}(E) e^{-(E_{mB}-E)/k_BT^*} \ , \tag{6}$$

where E_1 is the lower limit of the integration, and is discussed below. Since an individual defect is either in state A or state B, $N_B(t)$ and $N_A(t)$ are related by

$$N_D = N_B(t) + N_A(t) \ . \tag{7}$$

This condition implies that a fixed number (e.g., strained bonds or charged dangling bonds) of defects are determined by deposition conditions. These defects may or may not be part of the ensemble of the normally observed dangling bonds. This consideration is secondary to the relaxation analysis presented here. The annealed state is defined by $N_A(\infty) \gg N_B(\infty)$.

Defect annealing is generally a thermal process. Light-induced degradation usually exhibits a weak thermal activation near room temperature. Nevertheless, at high temperature ($> 100\,^{\circ}\mathrm{C}$), light-induced degradation is thermally activated with a high activation energy on the order of the annealing energy.[10,25]

For a thermally activated process, the transition rates are

$$W_{A\text{-}B}(E) = k_{ab} e^{-E/k_BT} \quad \text{and} \quad W_{B\text{-}A}(E) = k_{ba} e^{-E/k_BT} \ , \tag{8}$$

where k_{ab} and k_{ba} are the transition rate constants which depend upon the transition mechanism. For the two microscopic models of defect formation considered here, it is electrons or holes that cause the transition. Thus k_{ab} is a function of the carrier density. The annealing prefactor k_{ba} is on the order of a lattice vibration frequency ω.

If the energy for defect conversion is supplied by electron-hole pair recombination, this nonthermal process can be incorporated in the present model by assuming the following: (i) the absorbed photon transfers most of its energy into a local mode of the defect; (ii) the process can be characterized by an increase in local temperature to a value T_L. In this case I express the transition rate as $W_{A\text{-}B}(E)=k_L e^{-E/k_B T_L}$. The transition rate constant is k_L. I continue by considering only thermally activated transitions whose transition rates are given by Eq. (8).

To solve Eq. (6), the lower limit on the integration must be specified. States with low barriers have short conversion times. If the conversion time for these states is less than the minimum time ($t_{\min}$) in the measurement, these states remain in equilibrium throughout the entire measurement, and their change cannot be observed. The conversion time is related to the barrier height in the usual way, so that $t_{\min}=\nu^{-1}\exp(E_1/k_B T)$. This time separates those states that reconfigure during the measurement from those that remain in equilibrium. This gives physical meaning to ν, the "attempt to reconfigure" frequency which characterizes the ease of reconfiguration. It is the proportionality constant between the energy cutoff for the observable states and the time scale of the measurement. If ν is large, then only states with high barriers will take part in MSD relaxation. Conversely, if ν is small, low-energy barriers will be observed. Therefore, the minimum observable transition energy is related to $t_{\min}$ by

$$E_1=k_B T\ln(\nu t_{\min})\ . \tag{9}$$

Similar reasoning shows that defects with conversion times longer than $t_{\max}$, the longest experimental time, do not have a significant probability of making a conversion. Thus the maximum energy of the converted defects is related to $t_{\max}$ by $E_{\max}=k_B T\ln(\nu t_{\max})$. This will affect the value of E_{mB}. Consider that some process has driven the system of defects toward state B for a time $t_{\max}$. Thus only those states for which $E_{mB}\le k_B T\ln(\nu t_{\max})$ will be in state B. In equilibrium, the distributions have completely equilibrated, so that the maximum barrier heights will be determined by the structure of the material rather than the details of the conversion process.

The meaning of these energies in relation to the distribution of states is shown in Fig. 5. Only those states in the region between E_1 and $E_{\max}$ are observed. These are the states that relax during the measurement. Because of the exponential distribution of states, their number increases rapidly with degradation time. Therefore, more of the high-energy, harder to convert, states become metastable with longer degradation. Their number also increases exponentially with temperature. Those states that are hard to convert are hard to anneal. This is shown by the shaded region in Fig. 5. The region E_1 to $E_{\max}$ shows the population of state B for degradation for a certain time. Increasing the degradation time by Δt increases $E_{\max}$ by $k_B T\ln(\Delta t)$. These additional defects are shown by the shaded region in the figure. Because of the connection between conversion time and barrier height, those defects with highest-energy barriers will anneal last. If, in contrast, there were more defects with low-energy barriers, longer degradations would not produce an *observable* number of defects that are harder to anneal.

Various mechanisms can cause the transitions $A\Longrightarrow B$ and $B\Longrightarrow A$. In the weak-bond-breaking model, hole trapping in a bonding orbital is the first step of $A\Longrightarrow B$.[34,35] The bond-breaking activation energy is supplied by the subsequent electron-hole recombination. This implies that the recombination energy must be localized to the weak bond. However, the transition could also be thermally activated if the bond breaking is thermally assisted.

A charge-trapping reaction such as the Adler mechanism[22] involving charge capture plus thermal energy could also cause the transition. The barrier to the transition is the energy associated with the changes in bond angles as the defect relaxes to accommodate the new charge configuration.[58]

The integration in Eq. (6) is straightforward. As long as $\alpha=T/T^*<1$, the argument of the integral decreases exponentially at higher energy. Thus the lower limit dominates the integral. Performing the integration in Eq. (6) gives

$$\frac{dN_A(t)}{dt}=(-N_A(t)k_{ab}e^{-E_{mA}/k_B T^*}+N_B(t)k_{ba}e^{-E_{mB}/k_B T^*})\frac{e^{-(\Gamma E_1)}}{k_B T^*\Gamma}\ , \tag{10a}$$

where $\Gamma=1/k_B T-1/k_B T^*>0$. The time dependence of E_1 is explicitly shown by substituting Eq. (9) in Eq. (10a) to give

$$\frac{dN_A(t)}{dt}=[-N_A(t)k_{ab}e^{-E_{mA}/k_B T^*}+N_B(t)k_{ba}e^{-E_{mB}/k_B T^*}]\frac{(\nu t)^{\alpha-1}}{k_B T^*\Gamma}\ . \tag{10b}$$

Conservation of the total number of defects allows the solution of Eq. (10b) to be expressed in terms of either N_B or N_A using Eq. (7). The solution of Eq. (10b) for the number of defects in the degraded state B is

$$N_B(t)=\frac{N_D}{(1+\gamma)}+C_1 e^{-(t/\tau_r)^\alpha}\ , \tag{11}$$

where C_1 is a constant to be determined from the initial conditions, and

$$\gamma=\frac{k_{ba}}{k_{ab}}e^{-(E_{mA}-E_{mB}/k_BT^*)}, \tag{12}$$

which determines the population in the steady state. The defect relaxation time is

$$\tau_r=\nu^{-1}e^{+E_{\rm act}/k_BT}, \tag{13}$$

with

$$E_{\rm act}=k_BT^*\ln(\nu)+E_{\rm MN} \tag{14}$$

and

$$E_{\rm MN}=k_BT^*\ln(1-\alpha)-k_BT^*\ln(k_{ab}e^{-(E_{mA}/k_BT^*)}+k_{ba}e^{-(E_{mB}/k_BT^*)}) . \tag{15}$$

τ_r is the characteristic time for the defects to relax to steady-state conditions, and $E_{\rm act}$ is the thermal activation energy for this relaxation. The last term in Eq. (11) shows that any disturbance produces a stretched-exponential relaxation rather than a simple exponential relaxation. Equation (14) is just the Meyer-Neldel rule connecting $E_{\rm act}$ to the logarithm of ν, and is illustrated in Fig. 1.

Equations (11)–(15) can be used for annealing or production. Either $N_A(t)$ or $N_B(t)$ can be eliminated from Eq. (10) using Eq. (7). However, the initial conditions are different, and the rates k_{ba} and k_{ab} depend on the type of transition. The barrier energy E_{mB}, as discussed above, depends on the amount of degradation.

The steady state is reached when the annealing and production rates become equal. This condition is not often attained at room temperature because annealing is so slow. Nevertheless, steady-state conditions can be reached in minutes to hours at elevated temperature.[25] In the steady state, $dN_A(t)/dt=-dN_B(t)/dt=0$. Setting the right-hand side Eq. (6) to zero gives the following general relation between $N_A(\infty)$ and $N_B(\infty)$:

$$N_A(\infty)=N_B(\infty)\exp\left[-\frac{E_{mA}-E_{mB}}{k_BT}\right]\frac{k_{ba}}{k_{ab}} . \tag{16}$$

The steady-state population ratio in the two states is governed solely by the details of the transitions in either direction over the barrier and the difference in barrier heights. In this case, $E_{mA}-E_{mB}$ is just the difference in the ground-state energies. In thermal equilibrium in the annealed state it is reasonable to assume that $k_{ab}=k_{ba}$, so that the population ratio is given solely by the difference in the ground-state energies and the temperature.

I have demonstrated that defect-controlled relaxation is a general model which produces both stretched-exponential relaxation and a MN rule. I next apply this formalism to MSD annealing and production experiments. The two main microscopic models, weak-bond breaking and charge trapping, are discussed in the context of the DCR model of production and annealing. Finally, the DCR and HCR models are compared in order to point out their similarities and differences.

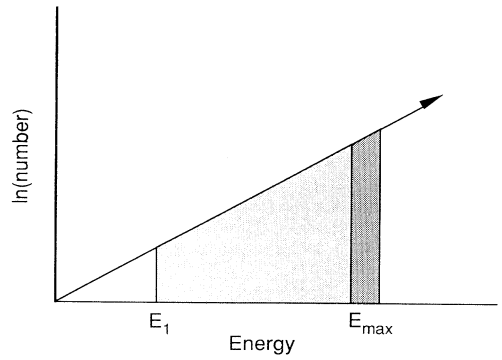

FIG. 5. Logarithm of the density of populated defects vs barrier energy. The solid diagonal line is the assumed exponential density of defects. The region between E_1 and $E_{\rm max}$ represents the defects observed in an annealing experiment.

III. COMPARISON WITH EXPERIMENT

A. Defect production

The expressions derived in Sec. II B can be applied to the thermally activated defect production observed for single charge injection as well as light-induced production at elevated temperature. They can also be used for nonthermal production, assuming the light raises the local defect temperature.

Equation (11) is used directly to find the time dependence of MSD production. Under illumination or during charge injection, $k_{ab}\gg k_{ba}$. Therefore, the transition rate from $A\Longrightarrow B$ is much larger than $B\Longrightarrow A$ and $\gamma\ll 1$. Thus

$$N_B(t)-N_B(0)=[N_B(\infty)-N_B(0)](1-e^{-(t/\tau_r)}) , \tag{17}$$

with the definitions for τ_r and $E_{\rm act}$ given by Eqs. (13)–(15), respectively. The constants $N_B(0)$ and $N_B(\infty)$ are the initial and steady-state densities, respectively. Equation (17) shows that the increase in defect density obeys, a stretched-exponential time dependence.

The activation energy for production is calculated using Eqs. (14) and (15). Since $k_{ab} \gg k_{ba}$, the last term in Eq. (15) can be neglected, and

$$E_{\rm act} = E_{mA} + k_B T^* \left[\ln(\nu) + \ln\left[\frac{(1-\alpha)}{k_{ab}} \right] \right] + \text{small terms} . \quad (18)$$

The leading term in $E_{\rm act}$ is E_{mA}, which shows that the activation energy is determined mainly by the maximum barrier height. However, there is a logarithmic correction to it that depends on the strength of degradation (i.e., the light intensity) through the transition-rate constant k_{ab}. Equation (18) demonstrates that production should obey a Meyer-Neldel rule. However, this has not yet been experimentally verified in the detail that it has for annealing.

The high activation energies observed from defect-production experiments made at elevated temperature show why thermally activated defect production does not compete with light-induced defect production near room temperature. The amount of thermally activated defect production to be expected at room temperature can be estimated from Eq. (17). The line in Fig. 1 relates ν to $E_{\rm act}$ if we assume that this relation also holds for production. Figure 6 is a plot of the time for 10% conversion from state A to B at various temperatures. Samples with typically $E_{\rm act} \approx 1$ eV convert slowly at room temperature. It takes about five days to convert 10% of the states, and two years to reach saturation. Since saturation of the Staebler-Wronski effect typically takes less than a year and 10% of the states can be converted in minutes, thermally activated conversion does not appear to be important at room temperature. Nevertheless, for defects with low activation energy, thermal conversion at room temperature is likely. For example, if $E_{\rm act} = 0.5$ eV, then 10% conversion takes less than an hour. Values of $E_{\rm act}$ below 0.6 eV are, however, usually associated with large concentrations of carbon.[59] In fact, it is the low $E_{\rm act}$ that makes degradation so easy in these materials. This is a serious problem for solar cells that use a carbon-based alloy for the p layer.[60]

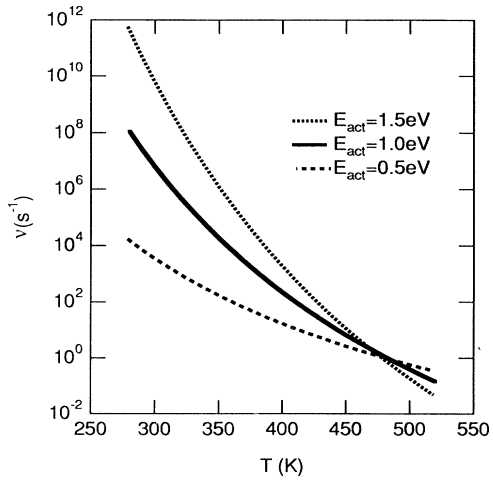

FIG. 6. Time for 10% conversion from state A to B vs temperature for different activation energies.

In Sec. II, I showed how the DCR model also explains nonthermal defect production by assuming that the absorbed photon transfers most of its energy into a local mode of the defect to raise the local temperature to a value T_L. A stretched exponential for defect production results by replacing T by T_L in Eqs. (10a) and (10b). However, the dispersion parameter becomes $\alpha = 1 - T_L/T^*$. A stretched exponential that mimics the $t^{1/3}$ law is obtained for $\alpha = \frac{1}{3}$. This gives a physical basis for the phenomenological arguments used by Redfield and Bube.[36] Testing this idea, however, requires careful experiment to determine whether or not α is a temperature-independent constant.

B. Defect annealing

All experiments show that MSD annealing is thermally activated. Therefore, Eq. (11) can be used directly for MSD annealing to give

$$N_B(t) - N_B(\infty) = [N_B(0) - N_B(\infty)] e^{-(t/\tau_r)^\alpha} , \quad (19)$$

with τ_r and $E_{\rm act}$ defined by Eqs. (13)–(15), respectively. The defect density reverts to its equilibrium value $N_B(\infty)$ with a stretched-exponential time dependence. $E_{\rm act}$ is the slope of an Arrhenius plot of $\ln(\tau_r)$ versus $1/T$. The annealing rate function ($S(t) = t[dN_B(t)/dt]$) which characterizes the distribution of annealing times for the MSD is maximized for $t = \tau_r(T)$.

An expression for the annealing activation energy can be obtained from Eqs. (14) and (15) with the assumption that $k_{ab} \approx k_{ba}$. These terms are expected to be on the order of a lattice vibration frequency ($\approx 10^{12}$ s^{-1}). Since $E_{mA} > E_{mB}$, the term containing E_{mA} in Eq. (15) can be neglected, and

$$E_{\rm act} = E_{mB} + k_B T^* \left[\ln(\nu) + \ln\left[\frac{(1-\alpha)}{k_{ba}} \right] \right] + \text{small terms} . \quad (20)$$

The leading term in $E_{\rm act}$ is E_{mB}. This shows that the activation energy is determined mainly by the maximum barrier height surmounted during degradation. In contrast, the activation energy for MSD production is determined by E_{mA} (see Sec. III A). Equation (20) is the Meyer-Neldel rule for MSD annealing.

Figure 1 shows a large range of annealing energies, covering a variety of measurements on all types of samples and devices. It is clearly inappropriate to refer to a single annealing activation energy in a-Si:H. The large range of activation energies arises from the Meyer-Neldel rule behavior. The large variation in "attempt to reconfigure" frequency produces the large range in annealing energies rather than any variations in E_{mB} with time of degradation.

Nevertheless, small changes in $E_{\rm act}$ can arise from the increase in E_{mB} with degradation time. The maximum energy of the states converted during degradation is es-

timated from arguments similar to those leading to Eq. (9) to give

$$E_{mB}=k_B T \ln(k_{ab} t_d) , \tag{21}$$

where t_d is the time of degradation. Substituting Eq. (21) into Eq. (20) shows how the activation energy and thus the annealing time constant depend on t_d. The longer the degradation time, the longer the annealing time. Similarly, the maximum of the annealing rate function will move to longer times.

The data in Fig. 3 reproduced from Ref. 49 for the change in the dark conductivity due to intense illumination are a good example of the increase in annealing time with longer degradation time. The number of defects converted also increases, as shown by the larger conductivity changes. The distribution of annealing times for conductivity relaxation can be found by computing the annealing rate function $[S_\sigma(t)=t(d\sigma/dt)]$ for the data in Fig. 3. This function is plotted in Fig. 7.

Figure 7 clearly shows that increasing the degradation time increases $S_\sigma(t)$ at long annealing times but leaves $S_\sigma(t)$ essentially unchanged at shorter times. $S_\sigma(t)$ is roughly proportional to the energy distribution of degradation-induced defects that are annealing at a time t. The data at short annealing times show that the number of defects with low barriers saturates after a brief degradation. However, it takes a longer degradation to convert the defects with higher barriers. Figure 7 also shows that there are more defects with higher barriers. Thus, these experimental results are best explained with a distribution of defects that increases exponentially with barrier energy, as sketched in Fig. 5.

Other experiments also support the prediction of increased annealing time with increased degradation time. Guha *et al.*[61] report that degradation at higher temperature produces defects that are harder to anneal. This implies that degradation is thermally activated and that higher temperature permits higher barriers to be surmounted. Other experiments show that longer degradation times at a fixed temperature produce recombination center density[62] and ESR spin signal increases[63] as well as solar cell[25] and conductivity[49] changes that are harder to anneal.

Figure 8 shows additional data demonstrating that longer degradation converts more defects with higher barriers. The change in open-circuit voltage (V_{oc}) in a *p-i-n* solar-cell monitors the number of MSD's. The annealing rate function $[S_{V_{oc}}(t)=t(dV_{oc}/dt)]$ is plotted versus annealing time in Fig. 8. The data clearly show the expected increase in the annealing-time constant with increasing degradation time. Nevertheless, the lengthening is not as much as predicted by Eq. (21). This relation would predict a thousandfold increase in the annealing time, whereas the experimental change is not much more than an order of magnitude. An explanation for this discrepancy is that the distribution of barrier heights increases less rapidly than for an exponential distribution. An additional example of annealing-time increases with degradation is found in Ref. 25, where the actual number of defects was determined directly from transient capacitance measurements.

C. *Meyer-Neldel rule from experiment*

Whenever the parameters ν and E_{act} are determined from an annealing experiment, they cluster along the Meyer-Neldel line, as shown in Fig. 1, indicating that all metastable phenomena in amorphous silicon obey the same MN rule. This result is consistent with the model presented in Sec. II, and shows that the underlying disorder of amorphous silicon giving an exponential distribution of defect barriers controls the annealing of metastable effects.

The parameters in Eq. (20), which describe the Meyer-Neldel relation for E_{act}, are determined from a linear regression fit to the data in Fig. 1. They are $E_{mB}=1.3$ eV

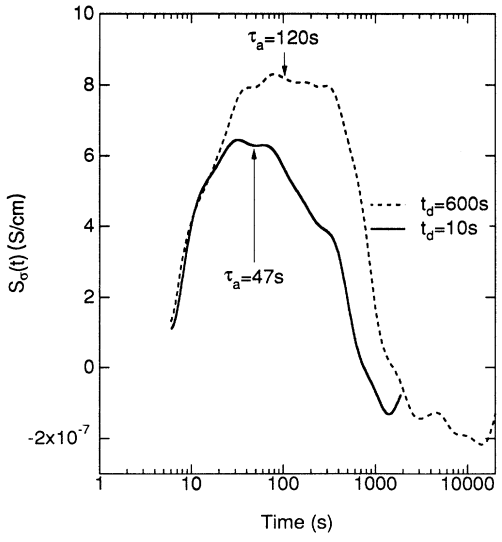

FIG. 7. The annealing rate function vs $\log_{10}(t)$ for the data shown in Fig. 3. The value of τ_A is the characteristic annealing time for the distribution. t_d is the time of degradation.

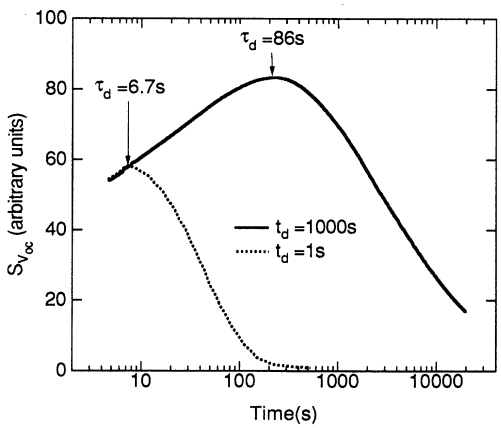

FIG. 8. $S_{V_{oc}}(t)$ for a *p-i-n* solar cell for two different degradation times at 359 K (from Ref. 25).

and $k_B T^* = 0.042$ eV. I assume that $k_{ba} \approx 10^{12}$ s^{-1}, a characteristic phonon frequency. The last two terms in Eq. (20) representing small corrections to E_{mB} are neglected. The value of $T^* \approx 490$ K is in excellent agreement with T^*, determined from the quench-in temperature for metastable defects in undoped a-Si:H.[62] The good agreement between these two values suggests that the distribution of defect barriers is frozen in at the same temperature as the other gap-state defects. The thermodynamic model of disorder-induced defects[26] predicts that all defect distributions are exponential and are determined by the same T^*.

Scatter in the data is expected, since E_{mA}, E_{mB}, and $k_B T^*$ can vary slightly among different samples and experiments. As Eq. (21) shows, scatter in E_{mB} due to changes in degradation time would be at most 0.1 eV. Variations among different samples could be larger.

IV. COMPARISON WITH MICROSCOPIC MODELS

In this section I compare the DCR model with the weak-bond breaking and charge-trapping models. I also compare annealing and production kinetics predicted by the DCR version of the weak-bond-breaking model and the charge-trapping model with predictions of the HCR model.

A. Weak-bond model

An assumption of the weak-bond-breaking model is that the energy to surmount the barrier $E_{A\text{-}B}$ is supplied by electron-hole recombination. However, the energy could also be supplied thermally. The potential barrier is assumed proportional to the strength of the weak bond, and likely decreases with the electronic energy difference between an "ideally bonded" valence-band electron and the valence-band-tail electron in the weak bond. The density of weak bonds decreases exponentially with energy above the valence band.[26]

McMahon and Crandall[64] measured a distribution of hole traps that could correspond to these weak bonds. They find a narrow distribution about 0.5 eV above the valence band. These hole traps disappear with intense illumination and reappear during annealing. In the weak-bond model, this would correspond to hole trapping followed by bond breaking to form dangling bonds which no longer function as traps. The first step is hole trapping in the weak bond, which is equivalent to exciting an electron from the bonding orbital.

If hole trapping is the precursor to weak-bond breaking, then there is competition between the weak-bond relaxation and thermal emission of the hole. Holes trapped at an energy E_s from the band edge are emitted at a rate $R_e \propto \exp(-E_s/k_B T)$. Thus the weakest bonds, farthest from the valence band, hold their holes longest and break with a probability proportional to R_e. Since R_e is thermally activated and the valence-band tail is exponential, the formalism in Sec. II can be directly applied to creation of defects in the weak-bond-breaking model.

Upon annealing, two T_3^0 defects reform the weak bond. Because the annealing activation energy is on the order of 1 eV, there must be a barrier to reforming the bond. Certainly, disorder will give a distribution of these barriers. By assuming that the distribution of barrier heights is exponential, the DCR model can be used and the arguments in Sec. II show that annealing will obey a stretched exponential and give a Meyer-Neldel rule.

The weak-bond model that includes hydrogen bonded to silicon[7,34,35] would fit equally well into the above framework. In this model, the Si—H bond moves to separate the dangling bonds. This bond movement presents a potential barrier with disorder giving a spread in barrier heights. This model is to be distinguished from the HCR model, in which the H is envisioned to diffuse, via bond breaking or insertion, to the weak-bond defect. In this HCR model, the bottleneck for both annealing and production is the *macroscopic* hydrogen movement away from the defect.

B. Charge trapping

Whenever a charge-sensitive measurement is used to study metastable defects, charge trapping or emission is observed. Transient capacitance measurements on Schottky barrier, p-n or p-i-n devices[10,25] and experiments with heterojunctions[12,33] all clearly indicate that charge change is associated with MSD formation and annealing. The measurements, however, do not distinguish whether charge change produces a charged or neutral defect, only that there is a change of charge on MSD formation. No one has directly measured whether this process accounts for the majority of the defects formed, nor whether the charge change produces spins measurable by ESR. The only evidence that dangling bonds are produced is indirect: the annealing and production kinetics are the same in both capacitance and ESR experiments. In solar-cell devices, capacitance changes (charge changes) are correlated with degradation of both the current and photovoltage.[25] The maximum number of charged defects that can be produced by illumination is about the same as the maximum number of spins or midgap defects produced in similar experiments.

Trapping of a charge (q) and the eventual conversion to a dangling bond requires the two steps represented by the reaction

$$T_3^q + (-q) \Longleftrightarrow (T_3^0)^* \underset{\text{relax}}{\Longrightarrow} T_3^0 \ . \tag{22}$$

The first part of the reaction shows the charge of $-q$ trapped by T_3^q to form the unrelaxed T_3^0 defect labeled $(T_3^0)^*$. The next step is relaxation to the stable dangling-bond defect. Since Si—Si bond angles must change during the relaxation process, there is a barrier to be overcome. The distribution of environments for these charged defects produces a distribution of barrier heights. Thermal emission of the trapped charge, at a rate R_e, competes with relaxation. Thus only those states farthest from the band edge retain their charge long enough for relaxation to take place. Since R_e is thermally activated, the formalism in Sec. II can be directly applied to defect creation by this general charge trapping reaction.

The result of McMahon and Crandall,[64] that holes trapped above the valence band convert to recombination centers on prolonged illumination, is most easily explained[27] in terms of the Adler model. The hole is trapped on a T_3^- defect forming a $(T_3^0)^*$ defect. Most of the time, the hole is thermally emitted to the valence band. However, occasionally the $(T_3^0)^*$ defect relaxes to form a stable T_3^0. Since the T_3^- is negatively charged, it is an excellent hole trap. However, once the hole is trapped, the center is neutral, making recombination with an electron unlikely. This is a "safe hole trap."[65]

Annealing is the reverse of reaction (22). The stable dangling bond relaxes to its original charged configuration.

In summary, thermodynamic arguments suggest that both charge trapping and weak-bond breaking or reforming take place over an exponential distribution of barrier heights. Thus annealing will obey a stretched exponential and give a Meyer-Neldel rule, in agreement with experiment. The two microscopic models both fit easily into the present DCR model. However, the charge-trapping model is consistent with more experiments. It best explains the fact that there are charge changes during MSD conversion. Similarly, the T_3^- is a better safe hole trap than the weak bond.

C. Comparison of HCR and DCR models

The HCR model[51] also gives a good fit to the data in Fig. 1. The stretched-exponential decay is of the form of Eq. (19), with a relaxation time given by an expression similar to Eq. (13). Analogous parameters take the same values when the data are analyzed with either the DCR or HCR models. For example, the distribution of hydrogen-bonding energies is an exponential of slope $k_B T^* = 0.42$ eV. This is the same value as the thermodynamic disorder in the DCR. The two models, based on quite different physics, explain the same set of data equally well using analogous parameters. The reason that both models give the same annealing and production kinetics is that the underlying disorder in the amorphous silicon is the main determinant of the form of the relaxation in each model.

One cannot use the Meyer-Neldel rule nor the fact that annealing follows a stretched exponential relaxation to test which model fits the data best. The good correlation between hydrogen transport and annealing of metastable effects is often cited as evidence that hydrogen is involved in MSD reactions.[51] However, since both models fit the annealing data, defect-annealing kinetics cannot be used as proof that hydrogen is involved in metastable defect relaxation.

The DCR and HCR models to differ, however, in a small term in the expression for the activation energy for annealing. In the HCR model,[51] the activation energy is

$$E_{\rm act} = k_B T^* \ln(\nu) + k_B T^* \ln\left[\frac{\alpha}{A D_{00}}\right], \tag{23}$$

where A is a constant and D_{00} a microscopic hydrogen-diffusion coefficient. Because this expression does not contain a term equivalent to E_{mb}, $E_{\rm act}$ does not depend on degradation time. The initial distribution of H atoms in their dispersive trapping sites is independent of the degradation time. Therefore, the annealing time should not depend on degradation time. However, as shown in Figs. 7 and 8, the annealing time clearly depends on degradation time.

In the DCR model, the physical reason for the increase of the annealing time with degradation time is that higher barriers take longer to surmount during degradation. Therefore, these high-energy barrier defects will not be observed for short degradation times. This would seem to favor the DCR model.

The HCR model predicts a single annealing energy of all metastable defects in a single sample of a-Si:H because there is only one pool of H controlling the kinetics. However, several experiments show more than one annealing energy for MSD in the same sample. An example of this is Fig. 7, where the MSD annealing shows two time constants. A short time constant of 47 s is observed for annealing of the conductivity decrease and a long time constant of about 120 s for annealing of the conductivity increase. Others[66] have also observed this behavior in thin films. In p-i-n devices, observation of two annealing times is common.[25]

These different annealing times have a natural explanation in terms of the charge-trapping model. Annealing of a T_3^0 by charge emission and relaxation to reform the original charged dangling bond would naturally be expected to occur on different time scales for the native T_3^- and T_3^+ defects. To anneal a T_3^0 to a T_3^+ defect requires emission of an electron to the conduction band; to anneal a T_3^0 to a T_3^- defect requires emission of a hole to the valence band. Since the T_3^0 levels are closer to the conduction band than the valence band, the activation energy for the former process is the smaller of the two. This is consistent with the experimental result that it is always easier to remove an electron than a hole from a MSD.

V. SUMMARY

Using a local model of defect-controlled relaxation in which the defect changes state *without* the aid of a diffusion atom, both the Meyer-Neldel rule and stretched-exponential annealing kinetics are explained. These results are due to an exponential distribution of activation barriers, which may be a natural consequence of the defects being frozen in during growth. It was shown that annealing energies (0.3–1.8 eV) from numerous metastability experiments lie along a Meyer-Neldel rule line. This model also predicts the same type of kinetics for thermally activated defect production. Furthermore, the activation energy for thermal production is higher than that of annealing, a result supported by experiment.[10,25] The expressions for stretched-exponential annealing and

the Meyer-Neldel rule are the same as those found for the HCR model based on hydrogen diffusion. The only distinction lies in the observed dependence of annealing time upon degradation time, a result which favors the present model over the HCR model. These models, based on different physical mechanisms, predict the same general behavior because they both reflect the underlying disorder of amorphous silicon.

ACKNOWLEDGMENTS

I wish to thank Howard Branz and Marvin Silver for many stimulating discussions about the topic of this paper. In addition, I appreciate Howard Branz's critical reading of the manuscript. This work was supported by the Department of Energy under Contract No. DE-AC02-83CH10093.

[1]The ("stretched-exponential") form of the time dependence is $\exp[-(t/\tau)^{\alpha}]$, where α is less than 1. See, e.g., D. G. Williams and C. Watts, Trans. Faraday Soc. **66**, 80 (1970).

[2]The Meyer-Neldel Rule is that the logarithm of the conductivity prefactor varies as the Fermi energy; see, e.g., W. Meyer and H. Neldel, Z. Tech. Phys. **12**, 588 (1937).

[3]J. Kakalios, R. A. Street, and W. B. Jackson, Phys. Rev. Lett. **59**, 1037 (1987).

[4]D. L. Staebler and C. R. Wronski, Appl. Phys. Lett. **31**, 292 (1977).

[5]H. Dersch, J. Stuke, and J. Beichler, Appl. Phys. Lett. **38**, 456 (1980).

[6]J. Pankove and J. E. Berkeyheiser, Appl. Phys. Lett. **37**, 705 (1980).

[7]K. Morigaki, I. Hirabayashi, and M. Nitta, Solid State Commun. **33**, 851 (1980).

[8]D. V. Lang, J. D. Cohen, J. P. Harbison, and A. M. Sergent, Appl. Phys. Lett. **40**, 474 (1980).

[9]D. L. Staebler, R. S. Crandall, and R. Williams, Appl. Phys. Lett. **39**, 733 (1981).

[10]R. S. Crandall, Phys. Rev. B **24**, 7457 (1981).

[11]D. V. Lang, J. D. Cohen, and J. P. Harbison, Phys. Rev. Lett. **48**, 421 (1982).

[12]A. R. Hepburn, J. M. Marshall, C. Main, M. J. Powell, and C. van Berkel, Phys. Rev. Lett. **56**, 2215 (1986).

[13]D. G. Ast and M. H. Brodsky, in *Physics of Semiconductors 1978*, edited by B. L. H. Wilson IOP Conf. No. 43 (Institute of Physics and Physical Society, London, 1979), p. 1159.

[14]W. B. Jackson and J. Kakalios, Phys. Rev. B **37**, 1020 (1988).

[15]P. E. Gruenbaum, R. A. Sinton, and R. M. Swanson, Appl. Phys. Lett. **52**, 1407 (1988).

[16]S. R. Elliot, Philos. Mag. B **39**, 349 (1979).

[17]D. L. Staebler and C. R. Wronski, J. Appl. Phys. **51**, 3262 (1980).

[18]M. Stutzmann, Philos. Mag. B **56**, 63 (1987).

[19]M. Stutzmann, Philos. Mag. B **60**, 531 (1989).

[20]A photon energy as low as 1.2 eV can produce MSD's. See, e.g., C. Y. Chen and Y. Huang, J. Appl. Phys. **62**, 2578 (1987).

[21]M. Stutzmann, W. B. Jackson, A. J. Smith, and R. Thompson, Appl. Phys. Lett. **48**, 62 (1985).

[22]D. Adler, Solar Cells **9**, 133 (1982).

[23]H. M. Branz and M. Silver, in *Amorphous Silicon Technology-1990*, edited by A. Madan, M. J. Thompson, P. C. Taylor, Y. Hamakawa, and P. G. LeComber MRS Symposiam Proceedings No. 192 (Materials Research Society, Pittsburgh, 1990), p. 267.

[24]H. M. Branz, Phys. Rev. B **39**, 5107 (1989).

[25]R. S. Crandall, Phys. Rev. B **36**, 2645 (1987).

[26]Y. Bar-Yam, D. Adler, and J. D. Joannopolus, Phys. Rev. Lett. **57**,467 (1988).

[27]H. M. Branz and M. Silver, Phys. Rev. B **42**, 7420 (1990).

[28]J. Ristein, J. Hautala, and P. C. Taylor, Phys. Rev. B **40**, 88 (1989).

[29]J. M. Essick and J. D. Cohen, Phys. Rev. Lett. **64**, 3062 (1990).

[30]T. Shimizu, H. Kidoh, A. Morimoto, and M. Kumeda, Jpn. J. Appl. Phys. **28**, 586 (1989).

[31]For a list of publications, see, e.g., H. M. Branz, Phys. Rev. B **38**, 7474 (1988).

[32]A. Chantre and D. Bois, Phys. Rev. B **31**, 7979 (1985).

[33]W. B. Jackson and M. D. Moyer, Phys. Rev. B **36**, 6217 (1987).

[34]M. Stutzmann, W. B. Jackson, and C. C. Tsai, Phys. Rev. B **32**, 23 (1985).

[35]M. Stutzmann, W. B. Jackson, and C. C. Tsai, Appl. Phys. Lett. **45**, 1075 (1984).

[36]D. Redield and R. H. Bube, Appl. Phys. Lett. **54**, 1037 (1989).

[37]H. Yamagishi, H. Kida, T. Kamada, H. Okamoto, and Y. Hamakawa, Appl. Phys. Lett. **47**, 860 (1985).

[38]C. Lee, W. Ohlsen, P. Taylor, H. Ullal, and G. Ceasar, Phys. Rev. B **31**, 100 (1984).

[39]N. Nickel, W. Fuhs, and H. Mell, Philos. Mag. B **61**, 251 (1990).

[40]C. Qui, W. Li, and D. Han, J. Appl. Phys. **64**, 713 (1988).

[41]S. Choi, B. Yoo, C. Lee, and J. Jang, Phys. Rev. B **36**, 6479 (1987).

[42]W. Tzeng, H. Tsai, and S. Lee, J. Appl. Phys. **62**, 1856 (1987).

[43]R. E. I. Schropp and J. F. Verwey, Appl. Phys. Lett. **50**, 185 (1987).

[44]J. Jang and C. Lee, J. Appl. Phys. **54**, 3943 (1983).

[45]J. Jang, T. M. Kim, J. K. Hyun, J. H. Yoon, and C. Lee, J. Non-Cryst. Solids **59&60**, 1804 (1983).

[46]J. Jang, S. C. Park, S. C. Kim, and C. Lee, Appl. Phys. Lett. **51**, 1804 (1987).

[47]H. Mell and W. Beyer, J. Non-Cryst. Solids **59&60**, 405 (1983).

[48]W. B. Jackson and J. Kakalios, Phys. Rev. B **37**, 1020 (1987).

[49]X. M. Deng and H. Fritzsche, Phys. Rev. B **36**, 9378 (1987).

[50]R. A. Street, C. C. Tsai, J. Kakalios, and W. B. Jackson, Philos. Mag. B **56**, 305 (1987).

[51]W. B. Jackson, Phys. Rev. B **38**, 3595 (1988).

[52]R. S. Crandall, in Ref. 29, p. 589.

[53]R. S. Crandall, J. Non-Cryst. Solids **114**, 597 (1989).

[54]M. Campos, J. A. Giacometti, and M. Silver, Appl. Phys. Lett. **34**, 226 (1979).

[55]J. C. Dyre, J. Phys. C **19**, 5655 (1986).

[56]H. R. Park, J. Z. Liu, and S. Wagner, Appl. Phys. Lett. **55**, 2658 (1989).

[57]Entropy changes can have a significant effect on transitions involving charged defects. See, e.g., H. M. Branz and R. S. Crandall, Appl. Phys. Lett. **55**, 2634 (1989).

[58]Fedders and Carlson show that T_3^0 changes its energy by 0.57 eV/deg upon relaxation. Therefore, on changing from T_3^0 ($sp3$) to T_3^- ($p3$) there is a 0.86-eV shift, and to T_3^+ ($sp2$) a

0.66-eV shift. See, e.g., P. A. Fedders and A. E. Carlson, Phys. Rev. B **39**, 1134 (1989).
[59]R. S. Crandall, D. E. Carlson, A. Catalano, and H. A. Weakliem, Appl. Phys. lett. **44**, 200 (1984).
[60]R. S. Crandall and D. L. Staebler, Solar Cells **9**, 63 (1983).
[61]S. Guha, C.-Y. Huang, J. Hudgens, and J. Yokomichi, Appl. Phys. Lett. **45**, 50 (1984).
[62]T. J. McMahon and R. Tsu, Appl. Phys. Lett. **51**, 412 (1987).
[63]M. Kumeda, H. A. Morimoto, and T. Shimizu, Jpn. J. Appl. Phys. **25**, L654 (1986).
[64]T. J. McMahon and R. S. Crandall, Phys. Rev. B **39**, 1766 (1988).
[65]T. J. McMahon and J. P. Xi, Phys. Rev. B **34**, 2475 (1986).
[66]J. Yoon, M. Kim, and C. Lee, J. Non-Cryst. Solids **114**, 636 (1989).